On the Validity of the Adiabatic Spreading Assumption in Droplet Impact Cooling

By

W.M. Healy
Building and Fire Research Laboratory
National Institute of Standards and Technology
Gaithersburg, MD 20899-8632 USA

J.G. Hartley and S.I. Abdel-Khalik
The George W. Woodruff School of
Mechanical Engineering
Georgia Institute of Technology
Atlanta, GA 30332-0405

Reprinted from the International Journal of Heat and Mass Transfer, Volume 44, October 2001, pp 3869-3881,

PERGAMON

International Journal of Heat and Mass Transfer 44 (2001) 3869–3881

International Journal of HEAT and MASS TRANSFER

www.elsevier.com/locate/ijhmt

On the validity of the adiabatic spreading assumption in droplet impact cooling

W.M. Healy [1], J.G. Hartley *, S.I. Abdel-Khalik

The George W. Woodruff School of Mechanical Engineering, Georgia Institute of Technology, Atlanta, GA 30332-0405, USA

Received 22 May 2000; received in revised form 2 January 2001

Abstract

The effect of heat transfer on the spreading of a water droplet impacting a heated surface has been numerically investigated. The aim is to assess the validity of commonly made assumptions in spray cooling models which ignore heat transfer during the droplet spreading period. The results of this study indicate that while the amount of heat transfer during the droplet spreading period may, itself, be small, its impact on the liquid coverage area and the subsequent heat transfer to the resulting liquid film may be substantial.

1. Introduction

The phenomenon of droplet impact on a solid surface has been studied extensively because of its applicability to a number of engineering processes. Spray coating, pesticide application, ink-jet printing, and spray cooling are among the applications in which understanding of the dynamics of liquid droplet impact could be used to improve the process. Of particular interest in the present study is the subject of spray cooling. Extremely high heat fluxes can be achieved through spray cooling, and the heated surface can be kept at a reasonably uniform temperature when wetted by a mist of liquid. A number of potential applications exist for spray cooling where the hot surface is below the minimum film boiling temperature, albeit still higher than the boiling point, of the sprayed liquid. Potential applications where high heat fluxes must be dissipated while the surface is kept at a relatively low temperature include high-power electronics, lasers, leading edges of aircraft, and nuclear reactor components during emergency conditions. Before predictions of the heat transfer to a spray can be determined, the fluid dynamics of a single droplet impacting a heated surface must be known.

In studying the heat transfer to a droplet during spray cooling, previous researchers have split the problem into distinct portions [1–6]. First, the droplet is assumed to spread adiabatically over the surface, resulting in a film shape for the subsequent heat transfer problem. After the film has completely spread, heat transfer is assumed to begin from the solid surface to the liquid drop. This approach appears to be reasonable when droplets impact surfaces that do not sustain boiling, since the spreading period is of the order of milliseconds while complete evaporation of the liquid film could take several seconds. The validity of this assumption and the associated error in the overall heat transfer rate, however, have not been examined. Considering the steep temperature gradients present upon impact, significant heat transfer may occur during this spreading stage. Additionally, a rise in the fluid temperature may affect the extent of spreading. Thus, simulating the fluid mechanics without heat transfer may lead to slight inaccuracies in the size and thickness of the film formed from these droplets, and hence, may impact the subsequent heat transfer rate.

Droplet impact has been studied extensively both experimentally and numerically. The review by Rein [7]

* Corresponding author. Tel.: +1-404-894-3248; fax: +1-404-894-8496.

E-mail address: james.hartley@me.gatech.edu (J.G. Hartley).

[1] Present address: National Institute of Standards and Technology, Building 226 Room B320, 100 Bureau Drive Stop 8632, Gaithersburg, MD 20899-8632, USA.

0017-9310/01/$ - see front matter
PII: S0017-9310(01)00041-2

Nomenclature

c	specific heat (J/(kg K))
g	gravitational acceleration (m/s^2)
k	thermal conductivity (W/(m K))
r	radial coordinate (m)
t	time (s)
u	velocity (m/s)
y	axial coordinate (m)
D	dissipation function
H	Heaviside function
R	initial droplet radius (m)
Re	Reynolds number
T	temperature (°C)
V	initial droplet impact speed (m/s)
We	Weber number

Greek symbols

α	thermal diffusivity of solid (m^2/s)
β	spreading ratio
δ	delta function
ϕ	level set function
κ	surface curvature (m^{-1})
μ	dynamic viscosity (kg/(m s))
θ	contact angle (deg)
ρ	density (kg/m^3)
σ	surface tension (N/m)
ξ	prescribed surface thickness (m)

Subscripts

film	liquid film
free	free-slip
s	solid
w	initial wall condition
i	initial fluid condition
max	maximum

Superscript

$*$	non-dimensional

summarizes many of the important aspects of the impact process. Photographic images of the process by several authors [5,8–13] display prominent features of droplet impact; the clearest pictures are given by Chandra and Avedisian [8]. When impact occurs on a heated surface, many interesting characteristics can be observed in the photographs. Chandra and Avedisian [8], Qiao and Chandra [5,9], Halvorson et al. [10], and Bernardin et al. [12,13] provide images of the boiling and evaporation of a droplet that impacts a heated surface. These images show that nucleate boiling occurs prominently in the rim of the liquid near the edge. These results indicate that the fluid dynamics create regions in the film which can sustain nucleate boiling while some regions are too thin to sustain nucleate boiling. Additionally, pressure variations in the liquid film due to the impact also affect bubble nucleation and growth. Hence, the impact dynamics may result in a highly non-uniform heat transfer rate over the wetted area. Bernardin et al. [12] also observed boiling in the liquid film before the droplet reached its maximum diameter on the solid, indicating that heat transfer during the spreading stage may be significant. This finding contrasts with conventional models of droplet evaporation that neglect heat transfer during spreading because the spreading stage is relatively short. The investigation of Bernardin et al., however, suggests that ignoring that heat transfer may lead to inaccuracies. To this end, this investigation has been undertaken. The aim is to quantify the amount of heat transfer during the droplet spreading period and assess the impact of such heat transfer on droplet spreading, and hence, the subsequent heat transfer through the liquid film.

To examine the effect of heat transfer during the spreading stage, a numerical model of the fluid mechanics and heat transfer has been used. Many researchers have previously solved the droplet impact problem numerically, starting with Harlow and Shannon [14] in 1968 with the Marker and Cell Technique (MAC). This technique used marker particles to indicate the presence of liquid; the method tracks the location of these particles as they are advected in the underlying velocity field. This technique, used recently by Hatta et al. [15], requires substantial computing power since the location of each particle needs to be stored and each particle is moved at every time step. To alleviate these computational problems, Hirt and Nichols [16] and Nichols et al. [17] developed the Volume of Fluid (VOF) Method. This method tracks the motion of a free-surface by introducing a new function termed the VOF function that indicates the fraction of a computational cell that is occupied by liquid. The VOF technique has been widely utilized to solve free-surface problems and is incorporated in several commercial codes. Specifically, the VOF method has been used successfully to study the droplet impact problem by several researchers [18–26]. Notable among these investigations is the recent work by Bussmann et al. [24] in which a three-dimensional model was used to simulate the impact of drops on a sharp edge and onto a plate angled at 45°. Much of the work has involved simulation of the simultaneous spreading and freezing of molten metal droplets. Few of the investigations, however, have examined the ramifications of heat transfer on the spreading of drops used for cooling applications.

Finite element techniques have also been used to study droplet impact problems. Fukai et al. [27–29] first introduced a technique to simulate molten metal droplets that placed elements only in the liquid portion and were thus able to obtain a large degree of resolution in the liquid. The results of this work show the importance of contact angle effects in the simulation. In the initial work, no particular treatment of contact line behavior was included, and the simulations of spreading did not qualitatively match the deformation of a liquid droplet. Inclusion of a contact angle and slip velocity in [28,29], though, made the results look physically realistic. Subsequent work by this group investigated the freezing of molten solder droplets on a substrate [30,31]. Bertagnolli et al. [32] also approached the problem using a finite-element scheme. Since finite-element schemes involve a higher degree of complexity and computational effort than Eulerian schemes, they were not chosen for this investigation.

A technique closely related to the VOF method is the level set method developed by Sussman et al. [33,34]. Instead of distinguishing the liquid region from the gas region using the discrete values of 1 and 0, the level set method uses a continuous distance function to indicate the distance from any point in space to the free-surface. The advection equation used for advancement of the level set function is identical to the one used to advance the VOF function. The authors performed thorough tests of this scheme, and validation of their methods can be found in [33,34]. Owing to its ability to accurately capture free-surfaces with simple algorithms, the level set code developed by Sussman et al. was selected as the starting point for the present investigation and will be described in further detail in the following section.

As mentioned in the previous discussion, droplet impact has been extensively studied through computer simulation. The aim of this work is not to present a new technique to simulate the phenomenon, but rather to use the techniques previously developed to examine the effect and extent of heat transfer during the spreading period itself. Such information will aid modelers of evaporation and boiling of this film in judging the accuracy of the model's predictions and underlying assumptions. While the two-dimensional axisymmetric model that has been used to study these effects is simpler than many existing techniques, it nevertheless provides an accurate representation of the spreading process to make valuable conclusions concerning the issue addressed in this investigation.

The purpose of the present work can be divided into three objectives. First, the effect of heat transfer from the impacted heated surface to the spreading droplet on the dimensions of the film formed by spreading is investigated. The dimensions are expected to change because viscosity and surface tension of the liquid are functions of temperature; the question, however, is whether such changes can be ignored. The effect of such changes can be seen in the simple analytical models of spreading discussed by Healy et al. [35]. These simple models assume constant surface tension and viscosity throughout spreading, but it is uncertain whether property changes from temperature variations in the liquid during the brief spreading stage are sufficient to have an appreciable effect on the spreading dimensions. The second goal is to determine the extent of heat transfer during the spreading stage. As mentioned previously, most analytical work on the evaporation or boiling of droplets on a heated surface ignores heat transfer during the spreading stage. This work aims to assess the validity of such an assumption. The third goal of the present work is to determine the extent of temperature change in both the spreading liquid and the solid on which the liquid impacts. Since images of droplet impact show distinct boiling regions, it is believed that the fluid dynamics of the impacting droplet may give rise to varying temperatures in the film, leading to regions with different heat transfer characteristics.

A numerical model utilizing the level set method has been used to solve the full Navier–Stokes equations coupled with the energy equation in the liquid and the conduction equation in the solid wall impacted by the droplet. The study will not examine phase change in the liquid as it spreads. It is assumed that the droplet is sufficiently small so that it is initially spherical and that the impact velocity, viz. the Weber number, is sufficiently low to ensure that the droplet remains intact upon impact. Water will be used as a representative fluid, and the initial solid surface temperature will be kept at the boiling point of water so that only single-phase heat transfer takes place at the solid–liquid interface. Several non-dimensional parameters that describe the spreading will be used in this study. The spreading ratio, $\beta = r_{\text{film}}/R$, is defined as the ratio of the radius of the spreading film to the initial radius of the droplet and gives a measure of the extent of spreading. The Weber number gives a ratio of the inertial effects of the droplet to surface tension effects

$$We = \frac{\rho V^2 (2R)}{\sigma}, \tag{1}$$

and the Reynolds number gives the ratio of the inertial effects of the droplet to viscous effects

$$Re = \frac{\rho V (2R)}{\mu}. \tag{2}$$

2. Formulation

The level set formulation solves the complete fluid equations over a rectangular domain as shown in the

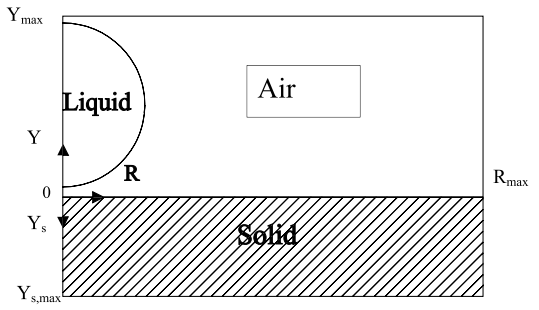

Fig. 1. Solution domain.

unhatched region of Fig. 1. The impact problem is axisymmetric, so that only half of the drop is seen in Fig. 1. The liquid and the surrounding gas are treated as one continuous fluid, and the level set function, ϕ, determines what properties are used in the governing equations. At all points in the domain, ϕ denotes the shortest distance to the liquid–gas interface. The level set function therefore has a value of zero along the interface, with values less than zero assigned to liquid and values greater than zero assigned to gas. The major benefit of such a tracking scheme is that the complex deformation of the free-surface can be captured on a fixed grid.

Sussman et al. [33,34] describes the formulation of the level set approach for solving problems in fluid mechanics in detail. Because focus of this work is on the results of simulations as opposed to the numerical method, only the basic approach developed by Sussman will be summarized, along with major modifications introduced in this investigation. The reader is referred to [33,34] for more detail on the level set method or to the references listed in the previous section to learn more about the details of simulating free-surface flow.

The governing equations are the full Navier–Stokes and continuity equations in incompressible form

$$\frac{\partial \vec{u}}{\partial t} + \vec{u}\cdot\nabla\vec{u} = -\frac{\nabla p}{\rho} - g\hat{y} + \frac{1}{\rho}\nabla\cdot(2\mu(T)D) + \frac{1}{\rho}\sigma(T)\kappa(\phi)\nabla H(\phi), \tag{3}$$

$$\nabla\cdot\vec{u} = 0. \tag{4}$$

The last term on the right-hand side of Eq. (3) applies surface tension forces as a body force according to the Continuum Surface Force (CSF) model [36]. In addition to these two equations, the following equation is used to advance the new variable, ϕ, in time:

$$\frac{\partial \phi}{\partial t} + \vec{u}\cdot\nabla\phi = 0. \tag{5}$$

To solve these equations, a second-order Runge–Kutta scheme is used to advance the variables in time. The viscous terms and surface tension terms are handled with conventional centered differencing, while the convection terms are treated with a third-order Essentially Non-Oscillatory (ENO) scheme [37,38]. The incompressibility constraint is applied through a projection method. Boundary conditions on the top and side boundary are maintained as no-penetration and free slip.

Some slight modifications to the analysis of the fluid mechanics are made in the present work. The no-slip condition is relaxed near the contact point where the liquid–air interface meets the solid. In this region, termed the contact region, slip is permitted to allow the liquid to spread along the surface. A similar technique was used with success by Fukai et al. [28]. This boundary condition is used to better simulate the motion of a contact line, especially in the early stages of spreading where fluid motion is dominated by inertial effects as opposed to surface tension effects. Without this treatment, a well-known stress singularity exists because the velocity gradient at the contact point approaches infinity if a no-slip boundary condition is applied. A smooth transition from free-slip at the interface to no-slip away from the interface is achieved by smoothing the region with a modified delta function and a pre-determined surface thickness, ξ

$$u = \xi[\delta(\phi)]u_{\text{free}}, \tag{6}$$

$$\delta(\phi) = \begin{cases} \frac{1}{2}[1+\cos(\pi\phi/\xi)]/\xi & \text{if } |\phi| < \xi, \\ 0 & \text{otherwise,} \end{cases} \tag{7}$$

where u_{free} is the free-slip velocity. This formulation of the delta function was developed by Sussman et al. to avoid step functions in properties and surface tension forces at the interface. While one prefers the value of ξ to be as small as possible to more closely simulate reality, it was found that a critical thickness was needed to assure stability of the scheme. In this work, ξ is set at 1.05 times the grid spacing in the r-direction. This value of ξ provides sufficient smoothing to prevent spurious oscillations at the interface yet yields a relatively thin free-surface region.

Heat transfer in the fluid is governed by a modified form of the energy equation

$$\frac{\partial(cT)}{\partial t} + \vec{u}\cdot\nabla(cT) = \frac{1}{\rho}\left[\frac{1}{r}\frac{\partial(rk(\partial T/\partial r))}{\partial r} + \frac{\partial(k(\partial T/\partial y))}{\partial y}\right]. \tag{8}$$

The lack of a subscript on T indicates that the temperature applies to the fluid. Dimensional analysis has shown that viscous heating is insignificant, and no heat generation occurs in the fluid. In Eq. (8), the specific heat, density and thermal conductivity in each medium are assumed to be constant. Over the temperature range

of interest, these properties of water change less than 10%. For air, the density and thermal conductivity change more significantly (near 20%), but this variation will be neglected since air plays a very minor role in the fluid mechanics and heat transfer in this problem.

The temperature field in the solid is governed by the conduction equation

$$\frac{\partial T_s}{\partial t} = \alpha\left[\frac{1}{r}\frac{\partial(r(\partial T_s/\partial r))}{\partial r} + \frac{\partial^2 T_s}{\partial y^2}\right]. \tag{9}$$

In Eq. (9), the thermal diffusivity is assumed to be independent of temperature. The presence of heat transfer also alters the fluid mechanics inasmuch as it may change the surface tension and liquid viscosity significantly enough so that the flow of the spreading droplet may be altered. Variable surface tension and liquid viscosity are included in the Navier–Stokes equations to capture these effects.

The boundary conditions for the heat transfer problem include insulated boundaries on the sides, constant temperature boundaries at the top of the fluid region and the bottom of the solid, and continuity of temperature and heat flux at the interface between the liquid and the solid.

2.1. Numerical scheme for heat transfer

Heat transfer calculations are performed after the new velocity field is found at a given time step. The energy equation in the liquid is first solved using the solid temperature at the fluid–solid interface as the boundary condition. This equation is solved using the same techniques used to solve the momentum equations. A second-order Runge–Kutta procedure advances the solution in time, a third-order ENO scheme is used to solve the convection terms, and central differencing is used for the conduction terms. After the temperature field in the fluid is obtained, the temperature field in the solid is calculated using the Alternating-Direction-Implicit (ADI) method. The boundary condition at the solid–liquid interface in this computation is taken as the continuity of heat flux at the boundary.

An additional stability constraint resulting from the inclusion of heat transfer in the numerical model arises from the conduction terms in the energy equation for the fluid. This constraint is [39]

$$\Delta t_T \leqslant \min\left[\frac{\rho(\phi)c(\phi)}{2k(\phi)((1/(\Delta r)^2) + (1/(\Delta y)^2))}\right]. \tag{10}$$

The convective term in the energy equation does not introduce a new stability constraint because it requires the same time step as the convective terms in the momentum equation. For the solution of the conduction equation in the solid, no time step restriction arises since the ADI method is theoretically unconditionally stable. In practice, it was found that the time step required for stable numerical modeling of the fluid was sufficient for modeling the heat transfer in the solid.

3. Results

In the present study, water is used as the liquid; accurate relations are available which give the variation of surface tension and dynamic viscosity with temperature. A regression was performed on the published property data [40] to obtain the following relations between properties and temperature:

$$\sigma = (0.07642) - (1.73 \times 10^{-4})T, \tag{11}$$

$$\mu = (4.419 \times 10^{-4}) - (3.057 \times 10^{-6})T + (0.013)/T, \tag{12}$$

where the units for σ are N/m, the units for μ are kg/(m s), and the units for T are °C. The fluid is assumed to have an initial temperature, T_i of 20°C while the initial solid surface temperature, T_w is assumed to be 100°C. This initial wall temperature value was chosen so that water will never exceed its boiling point, and hence, the onset of nucleate boiling will not occur. With the non-dimensional temperature defined as

$$T^* = \frac{T - T_i}{T_w - T_i}, \tag{13}$$

the initial non-dimensional fluid temperature is zero, and the initial non-dimensional wall temperature is unity.

Contact angles are assumed to be independent of temperature. Although several researchers have reported that contact angles vary with temperature [8,41], the variation has been found to occur primarily for temperatures above the boiling point. Below this temperature, the contact angle is relatively constant. Because all simulations are performed below the saturation temperature of water, a constant contact angle is used throughout this study.

To validate the performance of the CFD code, results from the numerical simulations were compared to experimental data on spreading from the literature [1,8,28,42–45]. Fig. 2 shows the numerical predictions plotted against the experimental values. Percent errors between the model predictions and the experimental results for the 27 data points obtained in the literature were computed. The model predicted β_{max} with a percent error of $-2.69\%\pm11.98\%$ using a coverage factor of 2 for the expanded uncertainty to approximate a 95% confidence interval.

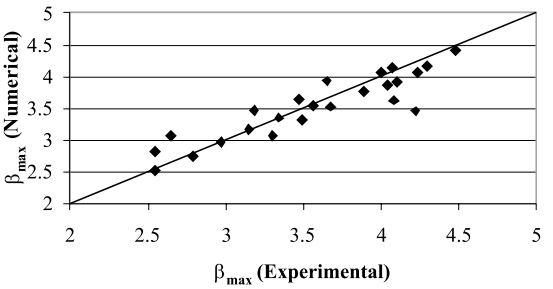

Fig. 2. Comparison of numerical predictions of β_{max} to experimental values.

The validity of the heat transfer model was more difficult to assess, owing to the lack of experimental data on temperature fields in the liquid and solid during spreading. To validate the code, predictions of heat transfer in the liquid and solid were separately compared to analytical predictions and were shown to match the analytical predictions of T^* within ± 0.005.

The schemes used are second-order accurate in both the time discretization and the spatial discretization. The major source of uncertainty in the results is the fact that mass is not conserved exactly by the scheme. For all simulations, it was ensured that the liquid mass did not change more than 5% from its initial value. Based on this value of mass change and other uncertainties in the computations, it is estimated that the uncertainty of the reported spreading ratios is $\pm 2.6\%$. The major uncertainty in the temperature calculations arises due to truncation error in the code. It is estimated that the expanded uncertainty in the calculations of T^* is ± 0.093, corresponding to an uncertainty of ± 7.0 K. Uncertainties in the heat transfer calculations are due to the temperature estimations. The uncertainty in heat flux has been estimated as ± 27 W/cm^2, and the uncertainty in integrated heat transfer predictions is ± 0.02 J. A coverage factor of 2 has once again been used in computing the previous uncertainties to approximate a 95% confidence interval.

To initially examine the effect of temperature on spreading, a water droplet with an initial radius, R, of 1 mm, an impact velocity, V, of 1.0 m/s, and a contact angle, θ, of 70° was examined. These impact conditions were selected to represent a characteristic case of droplet cooling and correspond to a Weber number value of 27.5 and a Reynolds number of 2000 when properties are evaluated at 20°C. A constant contact angle has been used throughout this study to isolate the effects of property variations in the liquid. Additionally, because this study is predominantly interested in the period up to the point when the maximum spreading ratio is attained, contact angle hysteresis is not considered. An accurate simulation of a receding film would likely require a receding contact angle that differs from the advancing contact angle, but recoil under a constant contact angle will be shown in results to show the behavior of the numerical model. While the true value of contact angle has a great deal of uncertainty, a value of $\theta = 70°$ has been used throughout the study as a representative value of the moderate contact angle. In examining the literature, one sees contact angles for water ranging from close to zero to values exceeding 100°. The 70° contact angle was selected based on the work done in [28] in which measurements of θ for water on glass and wax ranged from approximately 50° to 90°; the average of these extremes was used for this study. It should be noted, however, that the contact angle will differ for different situations. The value is highly dependent upon surface material and finish, may depend on the speed of the contact line, and is different for an advancing film than for a receding film. The reader is referred to [8,21,46–50] for a detailed discussion of the contact angle behavior.

3.1. Isothermal solid

Fig. 3 shows the transient spreading ratio versus dimensionless time ($t^* = tV/R$) for three cases of droplet impact. Curves are shown for droplets with constant properties evaluated at $T = 20$°C and $T = 100$°C. The third curve shows the spreading ratio for a water droplet with variable properties and an initial fluid temperature of 20°C impacting a surface that is maintained at 100°C. While the droplet with variable properties does not spread as much as the droplet with constant properties evaluated at 100°C, its maximum spreading ratio exceeds that of the droplet with properties evaluated at 20°C by 4.1%. Although this change in the spreading ratio may not seem dramatic, it causes a notable increase in the area covered by the liquid film. The area of this axisymmetric film is proportional to β^2, so the coverage area of the liquid increases by 8.3%. Since total heat transfer depends upon the area through which the heat transfer takes place, this example shows how the variation of viscosity and surface tension with temperature can affect the heat transfer to a film of liquid created by an impacting droplet.

The change in spreading ratio is more pronounced for cases with a higher spreading ratio because a greater proportion of the liquid in the droplet comes in contact with the hot surface. An example of such an impact occurs when the impact velocity in the previous example is increased to 2 m/s, so that the Weber and Reynolds numbers would increase to 110 and 4000, respectively, while the contact angle is assumed to remain unchanged at 70°. This case is representative of a high-inertia droplet impact in the impact regime considered in this study. Here, the spreading ratio is significantly higher for the case that includes heat transfer than for the isothermal case at 20°C. The β_{max} increases by 9.8%

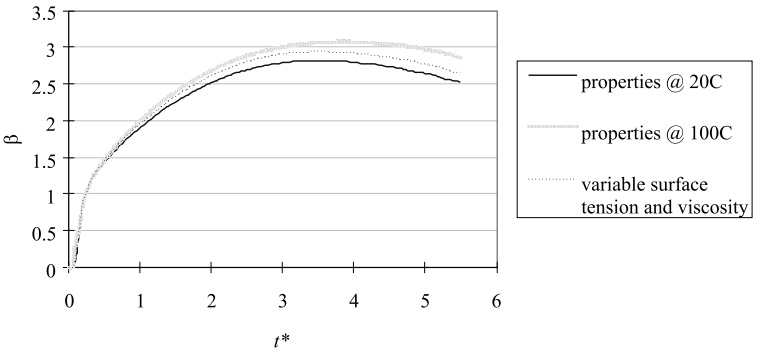

Fig. 3. Transient spreading ratio for impact onto an isothermal surface at 100°C compared to impact when properties are constant; $R = 1$ mm, $V = 1$ m/s, and $\theta = 70°$.

when heat transfer is present, leading to an increase of 19.6% in the coverage area of the liquid. This difference in spreading ratio is more pronounced than for the previous case because the higher impact velocity allows the film to spread more, thus subjecting more liquid to the hot wall. The increased coverage resulting from the high impact velocity allows the viscosity and surface tension to decrease considerably.

3.2. Solid surface with finite thickness

The droplet impact conditions used in the previous section are also used to evaluate the heat transfer from a solid with finite thickness. Surfaces with the thermal properties of aluminum and glass are considered in this study because they represent two solids with widely different thermal properties. Thermal properties are assumed to be constant because temperatures in the solid are expected to remain close to the initial temperature. Of interest in this study is the extent of temperature drop in the solid and any changes in the spreading that occur when a droplet falls on a surface that is not isothermal but is still at an elevated temperature. The final goal is to obtain better estimates of the heat transfer from the wall during the spreading stage.

The simulations start with the droplet just above the solid surface. The temperature throughout the fluid is set at $T_i = 20$°C, and the temperature throughout the solid is set at $T_w = 100$°C. Fig. 4 shows an example of the plots that will be shown. The length units on the axes are non-dimensionalized with respect to R. The solid line shows the droplet shape, while the dotted lines show contours at different non-dimensional temperature levels as indicated in the figures. Fig. 5 shows non-dimensional temperature contours in both the fluid and the solid at different times when a droplet with $R = 1$ mm, $V = 1$ m/s, and $\theta = 70°$ impacts a low-conductivity surface with the thermal properties of glass. These plots show that the air heats up rather quickly owing to its high thermal

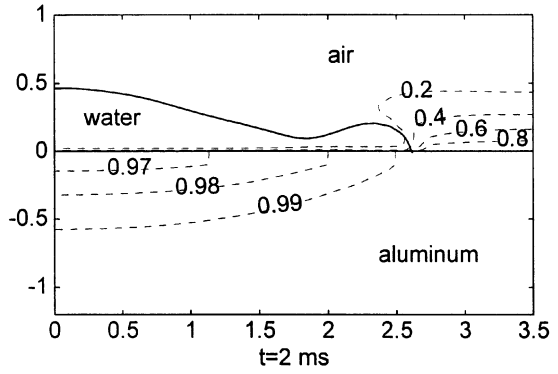

Fig. 4. Sample display of temperature contours within fluid and solid as the liquid spreads.

diffusivity, while the water temperature remains low for a longer time. As the droplet impacts the surface, heat transfer from the wall and air raises the liquid temperature slightly, but much of the fluid remains close to the initial droplet temperature. At $t = 5$ ms and $t = 6$ ms, a temperature rise can be seen in the liquid film in the region where it becomes thin. This temperature rise occurs because of the low thermal mass in this area. Because the film becomes very thin, the bulk temperature in this region approaches the saturation temperature of the liquid.

Temperatures in the solid fall significantly during the spreading stage. Near the surface, temperatures drop from $T^* = 1$ down to nearly $T^* = 0.6$. The contours at $t = 5$ ms show that the temperature in the glass drops markedly down to a non-dimensional depth of -0.1 ($= 0.1$ mm).

Fig. 6 displays the temperature contours in the fluid and the solid when a droplet with $R = 1$ mm, $V = 1$ m/s, and $\theta = 70°$ impacts a high-conductivity surface having the thermal properties of aluminum. It can be seen that

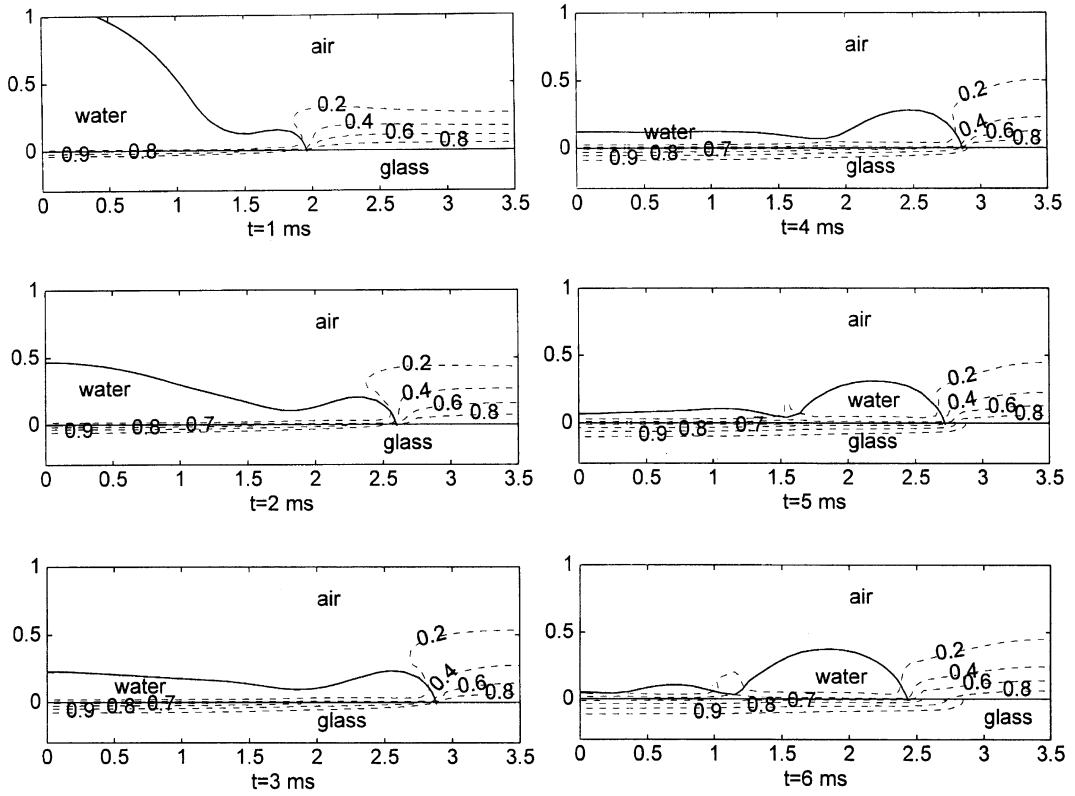

Fig. 5. Temperature contours when droplet with $R = 1$ mm, $V = 1$ m/s, $\theta = 70°$ impacts a surface with the thermal properties of glass (the length units on the axes are non-dimensionalized with respect to R).

the temperature field in the fluid is very similar to the previous case. The temperature drop in the solid, however, is minimal in this case because the thermal conductivity and thermal diffusivity of aluminum are large. Heat from within the solid readily conducts to the surface to maintain the temperature near the initial temperature. This result shows that impact onto a high-conductivity surface is nearly equivalent to impact onto an isothermal surface at the initial temperature of the solid.

Fig. 7 shows the transient spreading ratio for the impact conditions of $R = 1$ mm, $V = 1$ m/s, and $\theta = 70°$ onto both glass-like and aluminum-like surfaces compared to the spreading of a film at a constant temperature of 20°C. While impact onto a real glass surface would likely involve a different contact angle than impact onto an aluminum surface, the contact angles in these simulations are identical to isolate the effects of heat transfer on the spreading. (The following discussion refers to the surfaces as glass and aluminum to describe the thermal properties of the solid but not necessarily its surface wetting properties.) Despite the temperature reduction of the solid surface, the transient spreading ratio of the droplet in both cases still exceeds the spreading ratio for impact at 20°C. The spreading ratio is greater in the case where impact occurs onto an aluminum surface than onto a glass surface because more heat is transferred to the liquid by the aluminum surface than by the glass surface. Table 1 summarizes the results by comparing the maximum spreading ratios for the cases tested. One may observe that impact onto an aluminum surface yields nearly the same β_{max} as impact onto an isothermal surface at 100°C. While the spreading ratio does not increase as dramatically when the liquid impacts a glass surface, the change in β_{max} from the case where $T_w = 20$°C is still significant.

The simulations are used to assess the assumption used in several heat transfer analyses that the heat flux to the fully spread film is initially uniform [1–6]. The following discussion describes results that show that the heat flux from the solid to the liquid is actually quite non-uniform during the impact process. Fig. 8 shows the heat flux to the liquid at the solid surface at various spreading times for a droplet with $R = 1$ mm, $V = 2$ m/s, and $\theta = 70°$ impacting an aluminum surface; similar results are obtained when the droplet impacts a glass surface. The arrows show the approximate location of the contact point at the five times. This plot displays

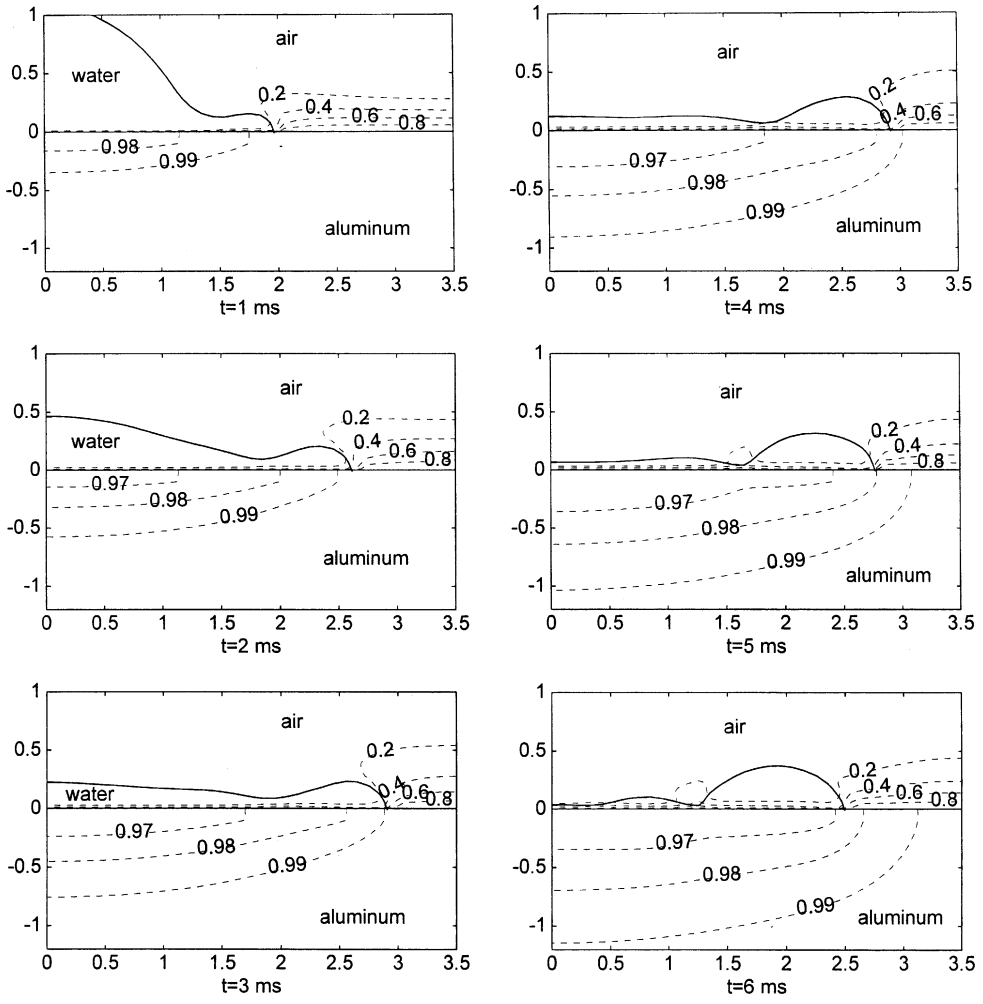

Fig. 6. Temperature contours when droplet with $R = 1$ mm, $V = 1$ m/s, $\theta = 70°$ impacts a surface with the thermal properties of aluminum (the length units on the axes are non-dimensionalized with respect to R).

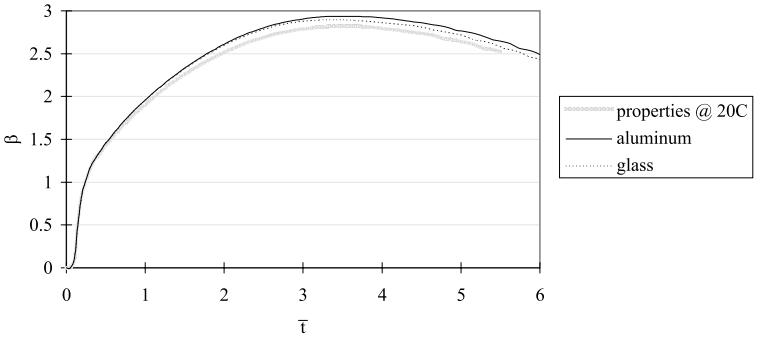

Fig. 7. Transient spreading ratios for impact onto glass and aluminum at $T_w = 100°C$ compared to impact onto a surface at $T_w = 20°C$; $R = 1$ mm, $V = 1$ m/s, $\theta = 70°$.

some critical aspects of heat transfer to a spreading film. The most noticeable feature is the sharp decrease in heat flux that occurs at the interface between the liquid and air. This result is expected since the heat transfer to air is negligible compared to heat transfer to the liquid. Another interesting aspect of these plots is the local

Table 1
Percentage increase in β_{max} from isothermal impact at 20°C

	Isothermal surface at 100°C	Aluminum surface at 100°C	Glass surface at 100°C
$R = 1$ mm, $V = 1$ m/s, $\theta = 70°$	4.1	4.0	2.7
$R = 1$ mm, $V = 2$ m/s, $\theta = 70°$	9.8	9.8	7.8

minimum in the heat flux near $r = 0.003$ m. The dip occurs where the liquid film becomes very thin and heats up considerably as shown by the temperature contours of Figs. 5 and 6. Because the liquid is at a high temperature in this region, less heat is transferred from the solid to the liquid. Closer to the liquid–solid–air interface, the heat flux begins to increase and reaches a maximum in close proximity to the contact line for times greater than 1 ms. This rise in the heat flux occurs for two reasons. First, the leading edge of the liquid encounters a solid that is always hotter than the solid under the center of the film. The second reason for the rise in heat flux is due to the liquid flow in this region. In the latter stages of spreading, the fluid in the contact region advances by a rolling motion, so the liquid near the contact point comes from the upper region of the liquid film rather than the wall region. The fluid circulating from the upper regions at the contact point is much cooler than liquid near the solid surface. The large temperature difference at this location causes the heat flux in this region to be greater than at other regions in the film. The difference in thermal mass from the non-uniformity in film thickness may also contribute to the variation in heat flux. The maximum heat flux is reached near the leading edge for times greater than 1 ms, and this value is nearly the same for all times plotted. Because temperatures of the liquid and wall remain relatively unchanged near the leading edge during the latter stages of spreading, the heat flux in this region remains steady.

Fig. 9 summarizes the total heat transfer results by showing the total heat transfer to the liquid from impact to the point of maximum spreading for the three wall conditions studied. The figure shows that heat transfer during impact onto an aluminum surface is very similar to the heat transfer from an isothermal surface, while the heat transfer to the liquid from the glass surface is slightly less than the other two cases. To give meaning to these numbers, it is useful to compare these values to the amount of heat required to raise the whole droplet from 20°C to 100°C (1.4 J). Fig. 9 shows that approximately 19% of this value occurs during spreading for the droplet with an impact velocity of 2 m/s on aluminum. According to these numbers, the heat transfer during the spreading stage may not be negligible when compared to the heat transfer necessary to evaporate the droplet. For the water droplet tested, the latent heat of vaporization is 9.5 J, so certain cases could yield heat transfer during spreading that accounts for several percentage points of the total heat transfer during evaporation of a liquid droplet.

3.3. Discussion

Images of a droplet spreading over a heated surface from a number of sources suggest that significant heat transfer may indeed occur during the spreading stage as displayed by these numerical results. Photographs from Chandra and Avedisian [8] of an *n*-heptane droplet impacting a stainless-steel surface at 104°C show nucleate boiling beginning in the region of the liquid film that has become thin. This finding agrees with the numerical result showing that the hottest part of the liquid film is the thinnest region. Halvorson et al. [10] and Bernardin et al. [13] provide additional images of a droplet im-

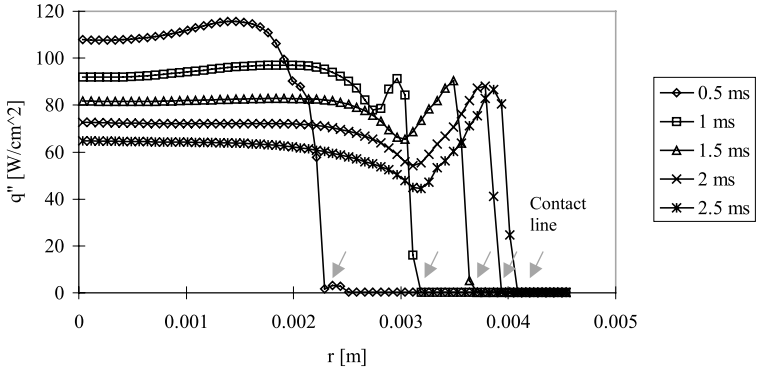

Fig. 8. Wall heat flux as a function of the radial position at different times after impact for droplet with $R = 1$ mm, $V = 2$ m/s, and $\theta = 70°$ impacting an aluminum surface.

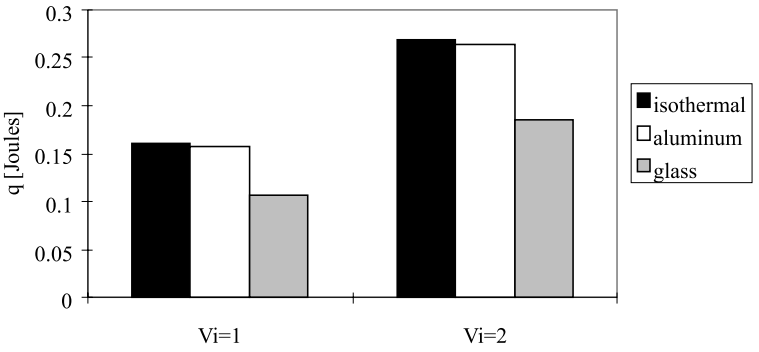

Fig. 9. Heat transfer to liquid during spreading for three different wall conditions.

pacting a heated surface, and both of these works showed nucleate boiling occurring in the rim of liquid formed during the late stages of spreading. Bernardin et al. also detected nucleate boiling in the film before the maximum spreading was reached when a water droplet impacted a polished aluminum surface at 125°C. All of these experiments indicate that the fluid dynamics create non-uniform heat transfer in the film. The outcome of these numerical simulations may help to explain the subsequent heat transfer to an evaporating droplet after impact onto a heated solid.

As mentioned previously, the value of contact angle used in this study was maintained at a constant value, but contact angles vary greatly in practice depending on factors such as material and impact velocity. While detailed simulations were not performed for contact angles other than 70°, one simulation worth noting was performed with a contact angle of 30°, an initial impact velocity of 1 m/s, and an initial droplet radius of 1 mm. In this instance, the maximum spreading ratio increased nearly 9% from the case with no heat transfer to the case where the solid surface was maintained at 100°C. This limited result suggests that the heating effect on spreading plays an even greater role when water droplets impact a hydrophilic surface. As in the case of higher impact velocity, it is suggested that the increased spreading time allows fluid properties to change more when the contact angle is smaller than when the contact angle is larger. This finding suggests that errors in predictions of heat transfer could be even more dramatic for droplets spreading with a small contact angle.

4. Conclusions

While it may appear reasonable to ignore any heat transfer during the spreading stage when computing the heat removed by a liquid droplet impacting a heated surface, some error is introduced in this assumption. While the overall heat transfer to the droplet during this time may, itself, be relatively small in comparison to the heat transfer during the evaporation process, the temperature rise in the fluid during spreading may cause changes in properties that lead to a significant increase in the spreading ratio. In this study, increases in the spreading ratio of nearly 10% were observed for a droplet impacting with a moderate speed onto a high conductivity surface. Ignoring temperature effects in this case may lead to a poor initial condition for the subsequent heat transfer analysis of the evaporation. Since the heat transfer rate to the liquid is a function of the film diameter, errors in predicted heat fluxes approached 20%. Such errors are decreased, however, as impact speeds decrease and diffusivity of the solid surface decreases.

In addition to the changes in spreading ratio, it was found that temperature gradients develop in the liquid film as spreading proceeds. Hot spots in the film could cause regions of boiling and evaporation while other parts of the liquid have not yet reached this condition. It was found that approximately 19% of the sensible heat needed to raise the droplet temperature to the saturation temperature was transferred from the solid to the liquid in the spreading stage when the droplet impacts a highly conducting surface. This effect and the change in spreading ratios when droplets impact a heated surface are possible sources of error in models that ignore heat transfer during the spreading stage and should be considered in future modeling of the droplet evaporation process.

References

[1] S. Toda, A study of mist cooling (2nd report: theory of mist cooling and its fundamental experiments), Heat Transfer – Jpn. Res. 3 (1974) 1–44.

[2] C.O. Pederson, An experimental study of the dynamic behavior and heat transfer characteristics of water droplets impinging upon a heated surface, Int. J. Heat Mass Transfer 13 (1970) 369–381.

[3] S. Inada, Y. Miyasaka, K. Nishida, Transient heat transfer for a water drop impinging on a heated surface (1st report, effects of drop subcooling on the liquid–solid contact state), Bull. JSME 28 (1985) 2675–2681.
[4] C. Bonacina, S. Del Giudice, G. Comini, Dropwise evaporation, J. Heat Transfer 101 (1979) 441–446.
[5] Y.M. Qiao, S. Chandra, Boiling of droplets on a hot surface in low gravity, Int. J. Heat Mass Transfer 39 (1996) 1379–1393.
[6] M. DiMarzo, P. Tartarini, Y. Liao, D. Evans, H. Baum, Evaporative cooling due to a gently deposited droplet, Int. J. Heat Mass Transfer 36 (1993) 4133–4139.
[7] M. Rein, Phenomena of liquid drop impact on solid and liquid surfaces, Fluid Dyn. Res. 12 (8) (1993) 61–93.
[8] S. Chandra, C.T. Avedisian, On the collision of a droplet with a solid surface, Proc. R. Soc. Lond. A 432 (1991) 13–41.
[9] Y.M. Qiao, S. Chandra, Evaporative cooling enhancement by addition of a surfactant to water drops on a hot surface, in: Proceedings of 1995 National Heat Transfer Conference, vol. 304, 1995, pp. 63–71.
[10] P.J. Halvorson, R.J. Carson, S.M. Jeter, S.I. Abdel-Khalik, Critical heat flux limits for a heated surface impacted by a stream of liquid droplets, J. Heat Transfer 116 (1994) 679–685.
[11] S. Chandra, C.T. Avedisian, Observations of droplet impingement on a ceramic porous surface, Int. J. Heat Mass Transfer 35 (1992) 2377–2388.
[12] J.D. Bernardin, C.J. Stebbins, I. Mudawar, Effects of surface roughness on water droplet impact history and heat transfer regimes, Int. J. Heat Mass Transfer 40 (1997) 73–88.
[13] J.D. Bernardin, C.J. Stebbins, I. Mudawar, Mapping of impact and heat transfer regimes of water drops impinging on a polished surface, Int. J. Heat Mass Transfer 40 (1997) 247–267.
[14] F.H. Harlow, J.P. Shannon, The splash of a liquid drop, J. Appl. Phys. 38 (1967) 3855–3866.
[15] N. Hatta, H. Fujimoto, H. Takuda, Deformation process of a water droplet impinging on a solid surface, ASME J. Fluids Eng. 117 (1995) 394–401.
[16] C.W. Hirt, B.D. Nichols, Volume of fluid (VOF) method for the dynamics of free boundaries, J. Comput. Phys. 39 (1981) 201–225.
[17] B.D. Nichols, C.W. Hirt, R.S. Hotchkiss, SOLA-VOF: a solution algorithm for transient fluid flow with multiple free boundaries, Los Alamos Report LA-8355, 1980.
[18] A.Y. Tong, B.R. Holt, Numerical study on the solidification of liquid metal droplets impacting onto a substrate, Numer. Heat Transfer A 31 (1997) 797–817.
[19] H. Liu, E.J. Lavernia, R.H. Rangel, Numerical simulation of substrate impact and freezing of droplets in plasma spray processes, J. Phys. D: Appl. Phys. 26 (1993) 1900–1908.
[20] W.-J. Chang, D.J. Hills, Sprinkler droplet effects on infiltration. I: Impact simulation, J. Irrigation Drainage Eng. 119 (1993) 142–156.
[21] M. Pasandideh-Fard, R. Bhola, S. Chandra, J. Mostaghimi, Deposition of tin droplets on a steel plate: simulations and experiments, Int. J. Heat Mass Transfer 41 (1998) 2929–2945.
[22] M. Pasandideh-Fard, Y.M. Qiao, S. Chandra, J. Mostaghimi, Capillary effects during droplet impact on a solid surface, Phys. Fluids 8 (1996) 650–659.
[23] G. Trapaga, E.F. Matthys, J.J. Valencia, J. Szekely, Fluid flow, heat transfer, and solidification of molten metal droplets impinging on substrates: comparison of numerical and experimental results, Metal. Trans. B 23 (1992) 701–718.
[24] M. Bussmann, J. Mostaghimi, S. Chandra, On a three-dimensional volume tracking model of droplet impact, Phys. Fluids 11 (1999) 1406–1417.
[25] H. Liu, E.J. Lavernia, R.H. Rangel, Numerical simulation of substrate impact and freezing of droplets in plasma spray processes, J. Phys. D: Appl. Phys. 26 (1993) 1900–1908.
[26] M. Kurokawa, S. Toda, Heat transfer of an impacted single droplet on the wall, ASME/JSME Thermal Eng. Proc. 2 (1991) 141–146.
[27] J. Fukai, Z. Zhao, D. Poulikakos, C.M. Megaridis, O. Miyatake, Modeling of the deformation of a liquid droplet impinging upon a flat surface, Phys. Fluids A 5 (1993) 2588–2599.
[28] J. Fukai, Y. Shiiba, T. Yamamoto, O. Miyatake, D. Poulikakos, C.M. Megaridis, Z. Zhao, Wetting effects on the spreading of a liquid droplet colliding with a flat surface: experiment and modeling, Phys. Fluids 7 (1995) 236–247.
[29] J. Fukai, Y. Shiiba, O. Miyatake, Theoretical study of droplet impingement on a solid surface below the Leidenfrost temperature, Int. J. Heat Mass Transfer 40 (1997) 2490–2492.
[30] Z. Zhao, D. Poulikakos, J. Fukai, Heat transfer and fluid dynamics during the collision of a liquid droplet on a substrate – I. Modeling, Int. J. Heat Mass Transfer 39 (1996) 2771–2789.
[31] J.M. Waldvogel, D. Poulikakos, D.B. Wallace, R. Marusak, Transport phenomena in picoliter size solder droplet dispension, J. Heat Transfer 188 (1996) 148–156.
[32] M. Bertagnolli, M. Marchese, G. Jacuccu, I.St. Doltsinis, S. Noelting, Thermomechanical simulation of the splashing of ceramic droplets on a rigid surface, J. Comput. Phys 133 (1997) 205–221.
[33] M. Sussman, P. Smereka, S. Osher, A level set approach for computing solutions to incompressible two-phase flow, J. Comput. Phys. 114 (1994) 146–159.
[34] M. Sussman, P. Smereka, Axisymmetric free boundary problems, J. Fluid Mech. 341 (1997) 269–294.
[35] W.M. Healy, J.G. Hartley, S.I. Abdel-Khalik, Comparison between theoretical models and experimental data for the spreading of liquid droplets impacting a solid surface, Int. J. Heat Mass Transfer 39 (1996) 3079–3082.
[36] J.U. Brackbill, D.B. Kothe, C. Zemach, A continuum method for modeling surface tension, J. Comput. Phys. 100 (1992) 335–354.
[37] C.-W. Shu, S. Osher, Efficient implementation of essentially non-oscillatory shock-capturing schemes, J. Comput. Phys. 77 (1988) 439–471.
[38] W. Mulder, S. Osher, J.A. Sethian, Computing interface motion in compressible gas dynamics, J. Comput. Phys. 100 (1992) 209–228.
[39] M.N. Özisik, Heat Conduction, Wiley, New York, 1993.

[40] R.E. Bolz, G.L. Tuve, Handbook of Tables for Applied Engineering Science, CRC Press, Boca Raton, FL, 1976.
[41] J.D. Bernardin, I. Mudawar, C.B. Walsh, E.I. Franses, Contact angle temperature dependence for water droplets on practical aluminum surfaces, Int. J. Heat Mass Transfer 40 (1997) 1017–1033.
[42] K. Tsurutani, M. Yao, J. Senda, H. Fujimoto, Numerical analysis of the deformation process of a droplet impinging upon a wall, JSME Int. J. 33 (1990) 555–561.
[43] J.A. Valenzuela, B.C. Drew, High heat flux droplet impingement heat transfer: Phase I Final Report, Technical Report TM-1190, Creare Inc., Hanover, New Hampshire, September 1987.
[44] R.E. Ford, C.G.L. Furmidge, Impact and spreading of spray drops on foliar surfaces, Wetting (1967) 417–432.
[45] M.H. Shi, J.C. Chen, Behavior of a liquid droplet impinging on a solid surface, Presented at 1983 ASME Winter Annual Meeting, 1983 (preprint #83-WA/HT/104).
[46] A.W. Adamson, Potential distortion model for contact angle and spreading II. Temperature dependent effects, J. Colloid Interface Sci. 44 (1973) 273–281.
[47] A.W. Adamson, Physical Chemistry of Surfaces, Wiley, New York, 1990.
[48] C. Budziak, E.I. Vargha-Butler, A.W. Neumann, Temperature dependence of contact angles on elastomers, J. Appl. Polym. Sci. 42 (1991) 1959–1964.
[49] A.W. Neumann, Y. Harnoy, D. Stanga, A.V. Rapacchietta, Temperature dependence of contact angles on polyethylene terephthalate, in: M. Kerker (Ed.), Colloid and Interface Science, vol. 3, Academic Press, New York, 1976, pp. 301–312.
[50] M.E. Tadros, P. Hu, A.W. Adamson, Adsorption and contact angle studies 1. Water on smooth carbon linear polyethylene and stearic acid-coated copper, J. Colloid Interface Sci. 49 (1974) 184–195.